THE PENNSYLVANIA STATE UNIVERSITY
COLLEGE OF ENGINEERING

SYSTEMS AND CONTROLS LABORATORY

RESEARCH REPORT NO. 12 UNIVERSITY PARK, PA. OCTOBER, 1970

THE SYSTEMS AND CONTROLS LABORATORY

The Systems and Controls Laboratory was started in 1964 to encourage graduate research and development on engineering systems, with emphasis on improving the understanding of basic elements and devices and bridging the gap between theory and practice. The experimental equipment and facilities of this laboratory have been provided for carrying out experimental investigations on devices and systems involving many of the different engineering disciplines. Staff members, graduate fellows, and graduate assistants are now working on projects and thesis topics of vital interest to engineers concerned with the advanced design and development of new engineering systems.

Much of the work involves mathematical and computer modeling and analysis and the experimental investigation of breadboard and prototype systems or devices. A major goal of this work is to accomplish a useful synthesis of analytical and experimental methods in research and development of advanced engineering systems for effective use by engineers and scientists working on future aerospace systems.

Financial support for this program is derived from the University, the National Aeronautics and Space Administration, and the Army Research Office. A major share of the projects in the Systems and Controls Laboratory are supervised by Dr. J. L. Shearer, Rockwell Professor of Engineering, and Dr. A. J. Healey, Assistant Professor of Mechanical Engineering, assisted by other members of the graduate faculty.

CONTENTS

THRUST MODULATION BY VORTEX GENERATION

T. D. Gillespie, Research Assistant in M. E.

This project, first mentioned in the Report of April 1967 [5], has now been completed. Its purpose was to investigate vortex generation as a means to modulate the thrust of reaction nozzles used on V/STOL aircraft. Subsequent reports [6-11]* describe the progress of the research, and the last shows the modulation effect to be predictable and considers its effectiveness as a thrust control mechanism.

The concept lends itself to application on simple reaction nozzles; although the general characteristics, which include modulation of mass flow rate along with the thrust, preclude application to jet engines without extensive design accommodation within the engine. Such an application only seems foreseeable when carried out at the manufacturer's level.

This project has provided graduate student support and the research has been used in a Ph.D. thesis entitled, "An Analytical and Experimental Study of the Influence of Swirl on Choked Nozzle Flow" [12]. The abstract of the thesis appears below.

ABSTRACT

"The introduction of swirl has been proposed as a way to modulate the flow rate and thrust of a reaction nozzle. Early experiments showed that introducing swirl into nozzle flow reduces the outflow rate. This investigation is concerned with the analytical and experimental study of the modulation under choked flow conditions.

"An analytical model is developed for an adiabatic, frictionless flow of uniform stagnation properties passing through a swirl generator in which all fluid takes on the same angular momentum per unit mass (potential vortex swirl distribution). The flow exhausts through a nozzle which converges so slowly that radial velocities are negligible (quasi-cylindrical assumption). The equations for conservation of mass, energy and angular momentum, the isentropic relationship, and the perfect gas equation are combined to relate the nondimensional mass flow rate per unit area to the ratio of specific heats, a swirl strength parameter, and the nondimensional axial velocity.

"By analogy to classical and polytropic nonrotating flow examples, the choking condition, where the flow rate becomes decoupled from the influence of downstream pressure, is shown to correspond to the maximum possible flow through a nozzle with fixed stagnation properties. In the more complex swirling flow case a graphical presentation is used to demonstrate the choking effect and to show that the choked mass flow rate is directly related to the throat swirl effect.

"The experimental program included a study of the throat flow conditions to permit evaluation of the throat swirl effect. Using measured throat distribution of flow direction, stagnation pressure, stagnation temperature and the throat wall static pressure, the throat velocity and pressure profiles were reconstructed. For this experimental equipment in which the swirl is generated by vanes in a vortex chamber preceding the nozzle, the reconstructed throat profiles show the potential vortex flow model to be a good approximation of the actual flow.

"Using throat swirl strength as the measure of the swirl effect, excellent agreement between the analytical and experimental results is obtained under choked flow conditions. Several points of disparity are observed and shown to be caused by the flow being unchoked despite the fact that the stagnation pressure was above that necessary for choking under nonswirling flow conditions.

"It is shown that given a choked nozzle without swirl, the introduction of swirl will reduce the mass flow rate. Should the swirl reach a sufficient magnitude, the flow may even become unchoked. Choking may be reinstituted by an increase in the ratio of upstream to downstream pressure."

This work was supported by NASA Grant No. NGL 39-009-023.

FLUID LINE DYNAMICS

R. R. Huber, Research Assistant in M. E.

A Master's thesis investigation of surges in liquid filled lines has been completed [13]. This investigation, described in previous reports [8, 9, 10, 11] involved comparing several simplified mathematical models with experimental data to evaluate the utility of the models. The experimental data obtained consisted of the recorded pressure transients observed in a long line after the rapid stoppage of various initial flow rates in the experimental line. As a second part of the investigation, analog simulation of the experimental line configuration was done using the digital delay simulator [5] in conjunction with an analog computer.

Pressures calculated using three different models were compared to the experimental data. These models were the constant exact RIC model (termed exact RIC model) [14], a simplified version of the exact RIC model (termed simplified RIC model) [15], and a model consisting of a distributed frictionless line with a lumped resistance at the upstream end (termed lumped-distributed models) [16]. The following recommendations on the use of these models were made:

1) For a line with a large resistance value, R, compared to the characteristic impedance at the line, Z_s, when the pressures and flow rates are needed at points other than the line end points, the exact RIC model should be used.

2) For a line with a large resistance value compared to the characteristic impedance of the line, when the pressures and flow rates are needed only at the line end points, the lumped-distributed model should be used.

3) For a line with a small resistance value, compared to the characteristic impedance of the line, when the pressures and flow rates are needed at points other than the end points of the line, the simplified RIC model should be used.

*Nos. in brackets denote references at end.

4) For a line with a small resistance value compared to the characteristic impedance of the line, when the pressures and flow rates are needed at only the line end points, either the lumped-distributed or a simplified RIC model can be used.

Several other conclusions about the entire investigation were also made:

1) The decay envelope of a surge as calculated using each of the three models, i.e., the exact distributed RIC model, the simplified distributed RIC model, and the lump-distributed model, can be made to closely fit the experimental decay envelope by choosing unsteady-flow resistances such that the experimental data and the models agree closely at a point near the tail-end of the transient.

2) The unsteady-flow resistance of the line is substantially greater than the steady-flow resistance of the line (also reported by Leonard [17]).

3) For the range of initial flow rates tested, 0.638 to 1.6 gpm, initially turbulent flow, the turbulence appears to dissipate rapidly and change to laminar flow after the closing of the valve. This lends support to the use of a laminar flow model to study water hammer of an initially turbulent flow as Leonard [17] did.

4) The digital delay simulator used in conjunction with an analog computer can be used to simulate line dynamics problems if the minimum resolution of the digital delay unit is small enough to handle the small changes in analog input signals properly.

This work was partly supported by NASA Grant NGL 39-009-023.

OPTIMIZER RESEARCH

R. W. Mayne, Graduate Fellow in M. E.

The purpose of this research has been to study the performance of relatively simple extremum control systems which may be realized using fluidic components and to construct a fluidic extremum controller suitable for maximizing prime mover performance via acceleration measurements. In Research Report No. 9 [9] the extremum control techniques most applicable to this problem were discussed. In Research Report No. 10 [10], the perturbation extremum controller using coincidence logic was analyzed, and in Research Report No. 11 [11], a fluidic perturbation optimizer was presented. The performance of a relay extremum controller has also been studied and part of the analysis will be discussed in this report.

A number of relay optimizer configurations have been considered in this investigation, but the one which has performed most satisfactorily (basically an approximation to the scheme proposed by Broekstra et al [18]) will form the basis for this discussion. The extremum controller has been studied in the prime mover simulation block-diagrammed in Fig. 1 of Report No. 10 [10] and by appropriate reduction, the diagram shown in Fig. 1 of this report may be obtained. This diagram is comparable to Fig. 2 of Report No. 10 [10] but represents the essentials of the relay optimizer rather than the perturbation optimizer. The gain κ is the lumped system gain.

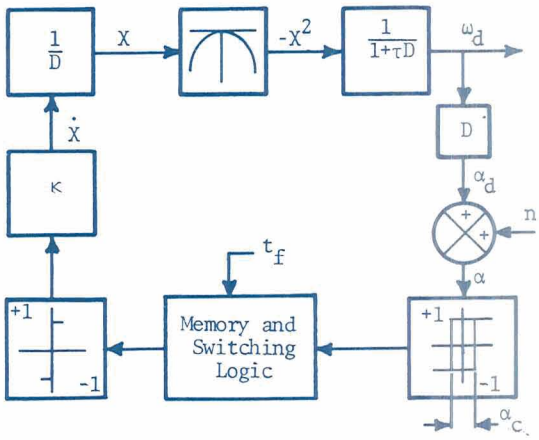

Fig. 1 The Relay Extremum Controller Acting on a Simplified System

The logic and memory unit of the relay controller has been shown as simply a black box in Fig. 1. Details of this part of the system are shown in Fig. 2 and t_f, the input to the unit shown in Fig. 1, is the period of forced switching oscillations produced by this controller through the action of the variable-width pulsers shown in Fig. 2. The logic and memory unit utilizes a comparator (signum sensor) yielding as its output a digital "1" for positive acceleration and a digital '0' for negative acceleration. When the acceleration changes from positive to negative, switching of the OR-NOR gate triggers the first variable-width pulser which changes the state of the output flip-flop and thus changes the state of the relay which controls the direction of adjustment of the parameter X.

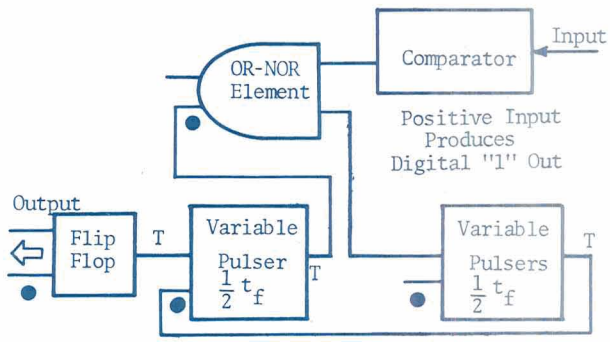

Fig. 2 Schematic of the Memory and Switching Logic

When the first pulser completes its cycle and turns off, it triggers a second pulser which is also an input to the OR-NOR. If the acceleration has become positive, when the second pulser turns off, no signal goes to the first pulser and the existing direction of parameter adjustment is maintained. However, if the acceleration is still negative, turn-off of the second pulser results in triggering of the first pulser, change of the flip-flop and relay state, and repetition of the preceding cycle producing a "forced" oscillation. The net result of the controller action is a reasonably smooth convergence of the parameter under control to its optimum value and a hunting cycle in the vicinity of the optimum value yielding maximum output speed in the prime mover application.

Study of the controller shown in Fig. 1 is generalized by nondimensionalizing the variables and parameters under consideration. The adjustable parameter X is replaced by

$$\Lambda = \frac{X}{K\tau}$$

and time is nondimensionalized with respect to the constant, τ, so that

$$T = \frac{t}{\tau}$$

These quantities then lead to other new variables

$$\dot{\Lambda} = \frac{d\Lambda}{dT} = \frac{1}{K}\frac{dX}{dt}$$

$$\Omega_{dr} = \frac{\omega_d}{K^2\tau^2}$$

$$A_{dr} = \frac{d\Omega_{dr}}{dT} = \frac{1}{K^2\tau}\alpha_d$$

$$A_{cr} = \frac{1}{K^2\tau}\alpha_c$$

and

$$T_f = \frac{t_f}{\tau}$$

Also, the noise n is set to zero for this discussion.

The results of the nondimensionalization are shown in the block diagram of Fig. 3, where it should be noted that the dimensionless loop gain is now simply unity. Performance of the system in Fig. 3 can be examined in terms of only two quantities, hysteresis magnitude, A_{cr}, and the forced switching period, T_f. Study of the controller on an Applied Dynamics Model 80 analog computer, combined with piece-wise linear analysis, has yielded the results presented herein.

A typical response of the relay optimizing controller is shown in Fig. 4 for the initial conditions $\Lambda = 5$ and $\Omega_{dr} = -25$. It can be seen that Λ approaches optimum with a speed $\dot{\Lambda} = 1$, overshoots and then gradually converges to its hunting zone, which in this $A_{cr} = 0$ case is defined by T_f and approaches zero as T_f approaches zero. The magnitude of the first overshoot seen in Fig. 4 is $\Lambda_{osr} = 1$ and it can be shown [19] that for other values of hysteresis the representative overshoot is

$$\Lambda_{osr} = \frac{1}{2}A_{cr} + 1$$

Thus, two of the primary performance characteristics for this optimizer have been readily established. The dimensionless correction speed $\dot{\Lambda} = 1$ is independent of both T_f and A_{cr} and the overshoot from any equilibrium initial condition which is appreciably off-optimum depends only on A_{cr} as mentioned above. Overshoot from nonequilibrium initial conditions may be considerably larger than $\Lambda_{osr} = 1/2\ A_{cr} + 1$; but for systems where the "static performance curve" has not undergone extensive upward shifts, the preceding discussion remains appropriate.

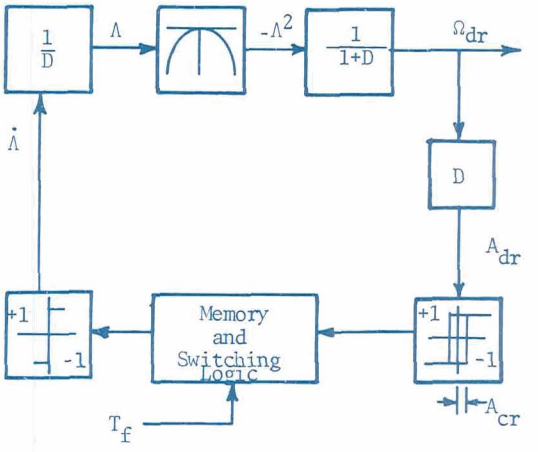

Fig. 3 The Nondimensional Relay Extremum Controller

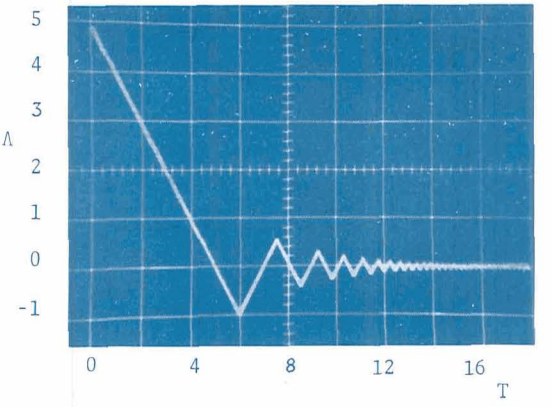

Fig. 4 Typical Time Response of the Relay Optimizer on Nondimensional Coordinates ($T_f = .1$, $A_{cr} = 0$)

The remaining performance characteristic to be considered is the steady state loss. In this discussion, the "hunting loss" is taken as the average value of Ω_{dr} in the steady state and is denoted by Ω_{Lr}. The hunting loss depends on both A_{cr} and T_f and Fig. 5 shows its typical dependence on T_f with $A_{cr} = .5$. It should be noticed that there is an optimum setting for T_f with a given hystersis magnitude. When T_f is below its best set point the system tends to drift slowly about optimum so that the maximum "average" hunting loss during this drift is more important than the actual time average hunting loss. Correspondingly, this "maximum" Ω_{Lr} is indicated in Fig. 5. For settings of T_f greater than the best value, the steady state limit-cycle is slightly displaced from optimum and is of rather large amplitude resulting in increased losses. The most desirable values of T_f for given values of A_{cr} are plotted in Fig. 6. The hunting losses obtained with the appropriate settings for T_f are shown in Fig. 7 as a function of A_{cr}. These results show essentially that

$$\Omega_{Lr} = - .85\ A_{cr}$$

which reduces to the dimensional result

$$\omega_L = - .85\ \tau\alpha_c$$

for the relay optimizer.

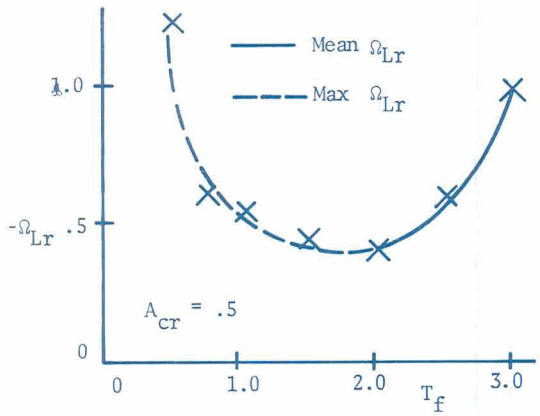

Fig. 5 Plot of Hunting Loss vs Forced Switching Time for $A_{cr} = .5$

The study above can be easily related to the study of the perturbation optimizer presented in the earlier report [10]. Expressions for response speed as a function of overshoot or response speed as a function of hunting loss can be determined which allow comparison of the two different optimizers. This comparison has been made for the hysteresis case considered in these reports and also for other sensing errors including bias and periodic disturbances as well as additional dynamic effects. Details of the comparison are shown in [19], but the net results are that the relay optimizer offers modest advantages for most "well behaved" systems but for systems where high frequency

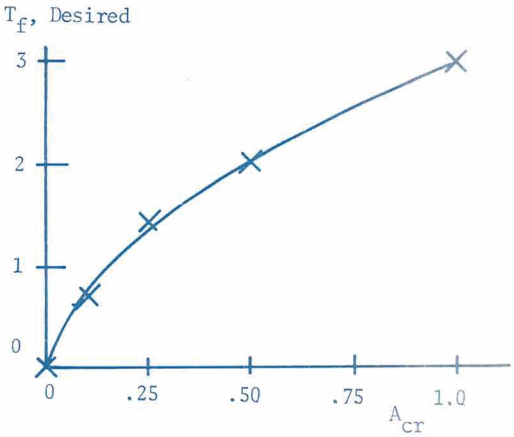

Fig. 6 Desired Forced Switching Time vs Hysteresis Magnitude

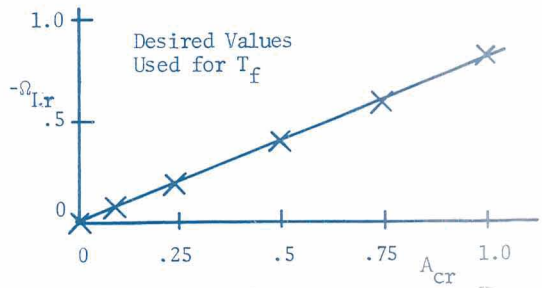

Fig. 7 Hunting Loss vs. Hysteresis Amplitude

disturbances are present or where sudden load changes resulting in upward motion of the static performance curve are common, the perturbation optimizer offers considerable advantage.

A Ph. D. thesis entitled, "Study of Simple Extremum Controllers Emphasizing Fluidic Implementation", is being submitted to the Graduate School and should be available early in 1971.

This work has been supported by an NDEA Fellowship at The Pennsylvania State University.

A THEORETICAL STUDY OF LAMINAR JET WALL REATTACHMENT

M. R. Fahnestock, Research Assistant in M. E.

Very basic to successful operation of a digital amplifier, whether turbulent or laminar, is the ability of the power jet to reattach to an adjacent solid wall. This phenomena has been studied in some detail by various investigators with the power jet operating in a turbulent regime. As far as is known to this investigator, the only effort that has included a theoretical study of laminar jet reattachment was the work by Comparin, Moore, and Jenkins [20]. Their analysis gave reasonable comparison to experimental results at higher wall angles (40° and 50°). The accuracy declined a bit at 30° and for 25° or less their analytical work gave a

negative slope which is physically impossible. It is the intent of this report to develop alternate relationships for reattachment distance and to extend the analysis to include wall offset as well as wall angle *. It will be seen that the theory does agree with the actual wall reattachment phenomenon for all wall angles, but the accuracy is woefully lacking at small angles. However, several empirical relations have been developed that provide a modified theory which gives results that compare quite favorably with all experimental data including that for small wall angles.

The model used to develop the theory for jet reattachment is shown in Fig. 8. The approach will generally follow the work by Levion and Manion [21] with the noted exception that this case involves laminar instead of turbulent reattachment . The following assumptions are customarily made and will be made in this analysis as well:

1) The jet emerging from the nozzle is two-dimensional and incompressible.

2) The centerline of the deflected or attached jet forms a circular arc of radius R.

3) The nozzle and jet widths are much less than the jet radius R.

4) The jet issues from the nozzle with a uniform velocity. The effect of reduced bubble pressure, in the separation bubble, on the jet discharge or velocity profile is neglected.

5) The jet is laminar and entrains surrounding fluid in a manner similar to that of a free jet. The deflection of, and the pressure gradients across, the jet do not affect entrainment.

6) The magnitude of the jet momentum along the jet centerline is conserved.

7) The pressure within the separation bubble is uniform.

8) Shear stresses in the fluid at the solid boundaries are negligible.

*The development will be given in more detail in the author's Masters thesis entitled, "Investigation of a Bistable Fluidic Amplifier Operating with Liquids at Low Reynolds Numbers", which will be available soon.

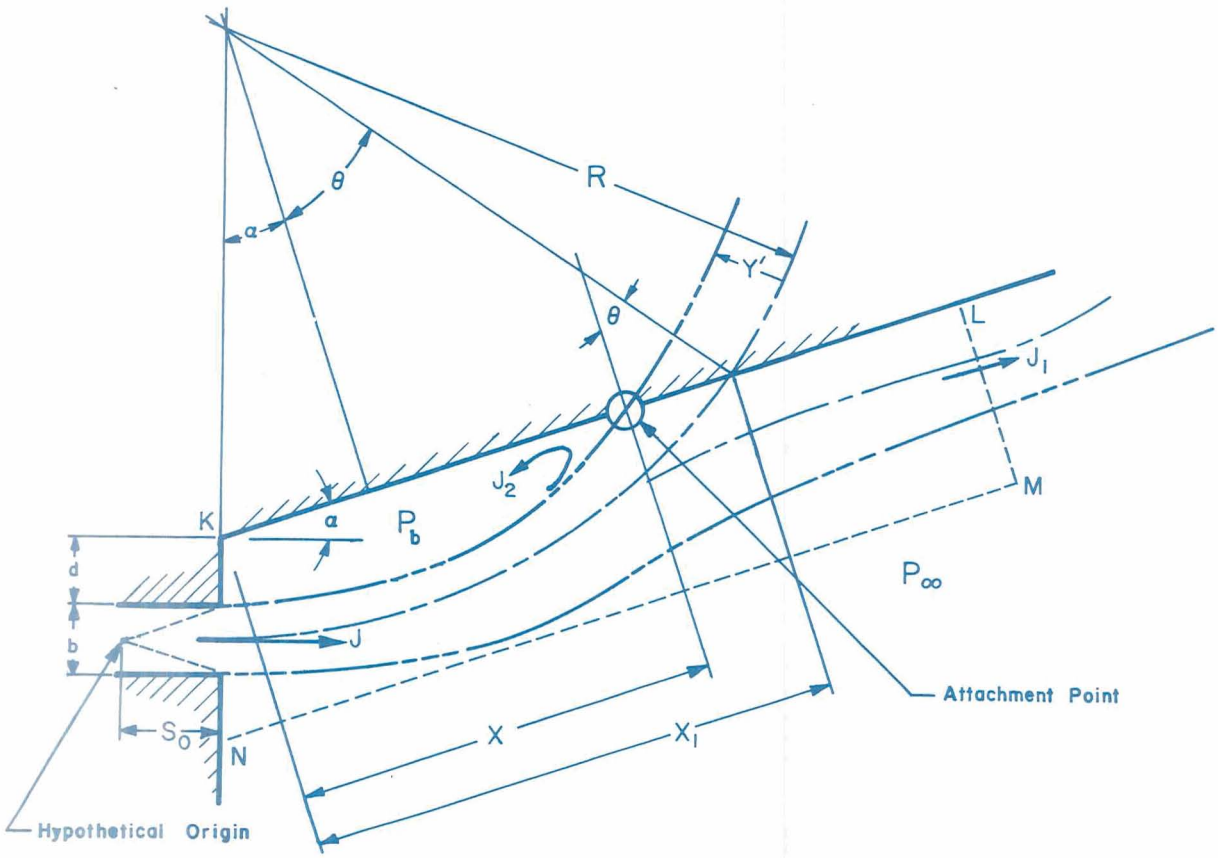

Fig. 8 Diagram Used to Develop Jet Attachment Model

The velocity distribution for a two-dimensional, free laminar jet is given by Schlicting [22] to be

$$u = \left[\frac{3J^2}{32\rho^2\nu(S+S_o)}\right]^{1/3} \operatorname{sech}^2\xi \qquad (1)$$

where

$$\xi = \left[\frac{J}{48\rho\nu^2}\right]^{1/3} \frac{y}{(S+S_o)^{2/3}} \qquad (2)$$

$$J = \frac{\rho V^2 b}{g_c} = R(P_\infty - P_b) \qquad (3)$$

g_c - gravitational conversion constant, 386 in./sec.^{2}

J - jet momentum flux, lbf/in.

ν - kinematic viscosity, in.^{2}/sec.

S - distance downstream along the jet centerline, in.

S_o - distance from the nozzle upstream to a hypothetical origin where the jet of momentum J issues from an infinitely thin slot (b→o), in.

R - Radius of curvature of ft. centerline, in.

V - average nozzle velocity of jet, in./sec.

y - distance from the centerline along the normal to the centerline, in.

ρ - fluid density, lb_m/in.^{3}

b - nozzle width, in.

When the jet reattaches to the wall, an attachment streamline is defined which extends from the edge of the nozzle to the point of attachment. For equilibrium conditions all the fluid entrained by the wall side of the jet must be returned to the separation bubble. Therefore, the attachment streamline can be described to contain between itself and the jet centerline a flow rate equal to one-half of the nozzle discharge and between itself and the wall a flow sufficient to satisfy its own entrainment. If y' is designated as the distance to the attachment streamline from the centerline, the velocity profile can be integrated to y' and the resultant flow rate equated to one-half the nozzle discharge flow rate. With a few simplifications, the equation for the attachment streamline can be obtained.

$$t'^3 = \frac{b}{36(S+S_o)} R_e \qquad (4)$$

where

$$t' \equiv \tanh\left(\frac{J}{48\rho\nu^2}\right)^{1/3} \left(\frac{y'}{(S+S_o)^{2/3}}\right) \qquad (5)$$

and R_e is the Reynolds number based on the nozzle width, b, and average velocity, V. The distance, S_o, to the hypothetical origin can be estimated by integrating the velocity in the nozzle exit plane where S = 0 and equating the integrand to the nozzle flow rate. The nondimensionalized result is

$$S_o/b = \frac{R_e}{36} \qquad (6)$$

A few geometric relationships, namely,

$$S = R(\theta+\alpha) \qquad (7)$$

and

$$\frac{d}{b} = \frac{R}{d}\left(1 - \left(\frac{\cos\theta}{\cos\alpha}\right)\right) \qquad (8)$$

combined with (4) and (6) give the dimensionless wall offset in terms of the dimensionless attachment streamline equation and the unknown jet attachment angle, θ, defined in the model. This wall offset is

$$\frac{d}{b} = \left(\frac{R_e}{36(\theta+\alpha)}\right)\left(1 - \frac{\cos\theta}{\cos\alpha}\right)\left[\frac{1}{t'^3}\right] - \frac{1}{2} \qquad (9)$$

The attachment distance, x, (nondimensionalized by the nozzle width) can be shown geometrically to be

$$\frac{x}{b} = \left(\frac{R-d-b/2}{b}\right)\sin\alpha + \frac{R}{b}\sin\theta - \frac{y'}{b\sin\theta} \qquad (10)$$

Equations (4) and (5) can be combined to yield

$$y' = \frac{2}{3t'^2}\tanh^{-1} t' \qquad (11)$$

and along with (4), (7) and (8), Eq. (11) can be substituted into (12) to give a relationship for the nondimensionalized attachment distance

$$\frac{x}{b} = \frac{R_e}{36(\theta+\alpha)}\left[\frac{1}{t'^3} - 1\right](\sin\alpha - \sin\theta) - \left(\frac{d}{b} + \frac{1}{2}\right)\sin\alpha - \frac{\tanh^{-1}t'}{3t'^2\sin\theta} \qquad (12)$$

If a relationship between the streamline equation (t') and the jet attachment angle (θ) can be determined, Eq. (12) can be used to predict the attachment distance, along with the contribution from Eq. (9), the wall offset. There exist two methods by which this relationship can be determined, both involving momentum considerations. The first to be considered is a balance of momentum flux locally about the point of attachment and will be referred to as the attachment point model. The attachment point model is made possible through the assumption that no jet momentum is dissipated. It does neglect the pressure contribution from the reattachment bubble. The model is derived from the simple relationship

$$J_1 - J_2 = J\cos\theta \tag{13}$$

By integrating over the velocity profile, the individual momentum terms can be found.

$$J_1 = \int_{-\infty}^{y'} \rho u^2 dy = \frac{3}{4} J\left(\frac{2}{3} + t' - \frac{1}{3}t'^3\right) \tag{14}$$

$$J_2 = \int_{y'}^{+\infty} \rho u^2 dy = J\left[\frac{1}{2} - \frac{3}{4}\left(t' - \frac{1}{3}t'^3\right)\right] \tag{15}$$

where t' is defined in Eq. (5). Combining Eqs. (13), (14), and (15) gives the desired relationship between attachment angle θ and the parameter t':

$$\cos\theta = \frac{1}{3}\left(3t' - t'^3\right) \tag{16}$$

The second method is a control volume approach. The control volume is shown in Fig. 8 and is bordered by the perimeter K-L-M-N. The basic assumption is that the reattachment bubble pressure is constant at some mean bubble pressure, P_b, and changes discontinuously at the jet centerline to the surrounding pressure, P_∞. This mean bubble pressure is by definition the pressure acting on the control volume side K-N. The control volume momentum equation becomes

$$J\cos\alpha - J_1 = (P_\infty - P_b)\left(d + \frac{b}{2}\right)\cos\alpha \tag{17}$$

Equation (17) can be combined with the geometric identity

$$R\cos\theta \equiv \left[r - \left(d + \frac{b}{2}\right)\right]\cos\alpha \tag{18}$$

and

$$\frac{J}{R} = (P_\infty - P_b) \tag{19}$$

to show that

$$\cos\theta = \frac{J_1}{J} \tag{20}$$

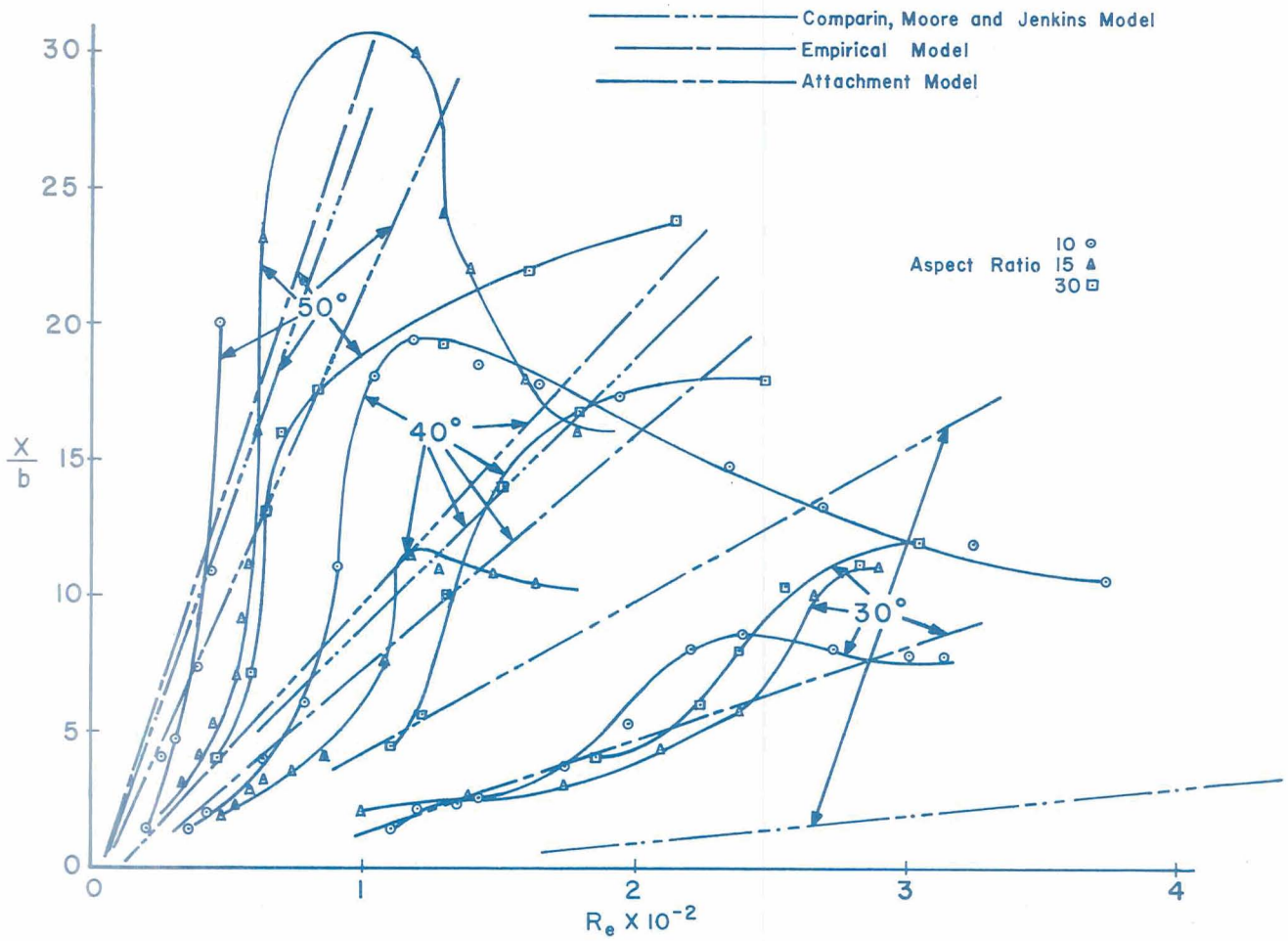

Fig. 9 Comparison of Attachment Point and Empirical Models to Experimental Attachment Distances

Equation (14) can now be substituted and the result is the control volume t' - θ relationship

$$\cos\theta = \frac{1}{2} + \frac{1}{4}(3t' - t'^3) \qquad (21)$$

Equations (9), (12) and (16) or (21) can now be used to predict the nondimensionalized reattachment of a laminar power jet for various geometric configurations. There is one major shortcoming, however, to the theory; the jet reattachment angle, θ, remains indeterminate. This is true for turbulent reattachment as well, and the customary procedure for circumventing the problem is to assume that θ is approximated by α, the wall angle. This is generally the case for large wall angles (greater than 25°), but not at all to be expected for small angles. None-the-less, if it is assumed to be true, the equations can be solved and the results are graphed in Figs. 9 and 10. The experimental attachment distances are taken from a paper by Comparin, Moore, and Jenkins [20]. The data in only for zero wall setback.

At the outset it is noted that the theory predicts a linear relationship between laminar jet reattachment angle and jet Reynolds number. The experimental data indicates this is a fair approximation of the actual phenomena.

Secondly, the predicted attachment distance using the control volume model is omitted from the graphs. The simple reason is that this model grossly over-estimated the attachment distance. The most likely reason for this inaccuracy is the assumption of a constant bubble pressure. Also, it can be expected that the accuracy of this model would decrease as the wall angle and/or wall setback decreases.

The attachment point model gives good agreement at wall angles of 40° and 50°, fair agreement at 25° and 30°, becomes increasingly poor at 20° and relatively little comparison at the smallest angle of 15°. The poor results at smaller angles are generally due to the fact that the deflected jet centerline is not really circular in shape at these small angles. Additional error stems from the nearness of the solid wall because of no setback and small angle. The entrainment and velocity profiles assume a free jet and the near wall certainly induces an adverse effect on this assumption.

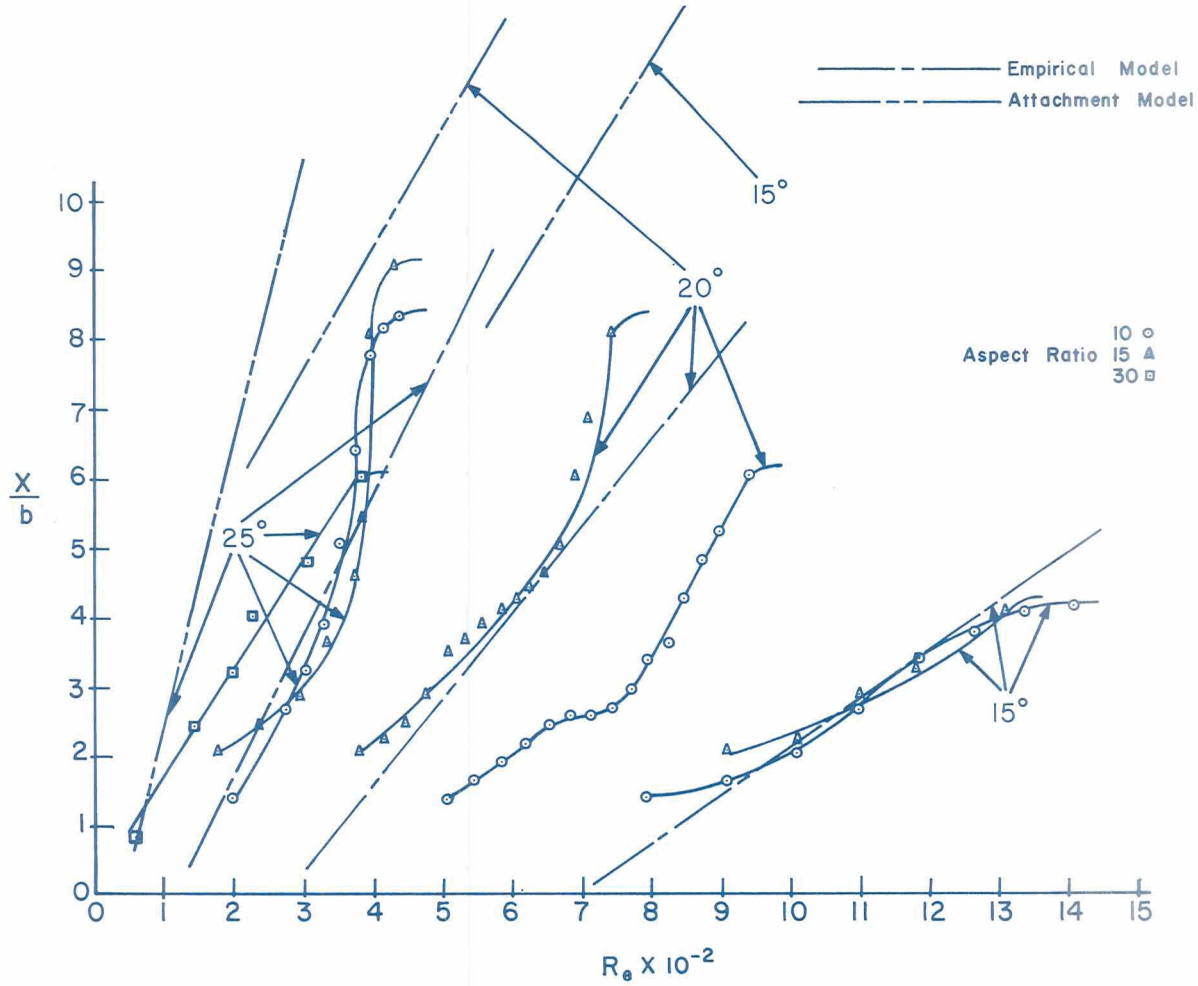

Fig. 10 Comparison of Attachment Point and Empirical Models to Experimental Attachment Distances

However, the major drawback to both the attachment point model and the control volume model is still the indeterminate jet reattachment angle which is particularly troublesome at the small wall angles. Hence, the unmodified theory can hardly be applied to fluidic devices where small wall angles are commonplace. To bring the predicted results more in line with the actual results, several empirical relationships were developed. The first two empirical forms retained all relationships developed previously, and simply determined an additional relationship for the jet attachment angle. These empirical forms were developed via use of the digital computer. For the empirically improved attachment point model

$$\theta = 1.22\alpha - 11.6 \qquad (22)$$

and for the improved control volume model

$$\theta = 0.84\alpha - 8.05 \qquad (23)$$

A third form developed again assumed the angles in question approximately equal and instead revised the θ versus t' relationship found through the simplified momentum considerations. This produced

$$\cos\theta = 0.39 + 0.64t' \qquad (24)$$

The predicted attachment distances are shown plotted on Figs. 11 and 12. It is seen that all empirical forms give good agreement with the actual throughout the range studied with the empirical θ versus t' form giving best comparison. The significance of these forms is not that the jet attachment angle is a function only of wall angle for surely it is not. Instead, the accumulation of errors resulting from all the assumptions seems to be influenced fairly directly by the wall angle. The good comparison indicates that for the basic geometry studied the attachment distances for intermediate angles could be confidently predicted. As for other configurations a similar approach might give improved results; and, coupled with experimental work, empirical forms might be developed that would enhance the theory.

This work was supported by funds from NASA Grant NGL 39-009-015 to the Space Science and Engineering Laboratory at The Pennsylvania State University.

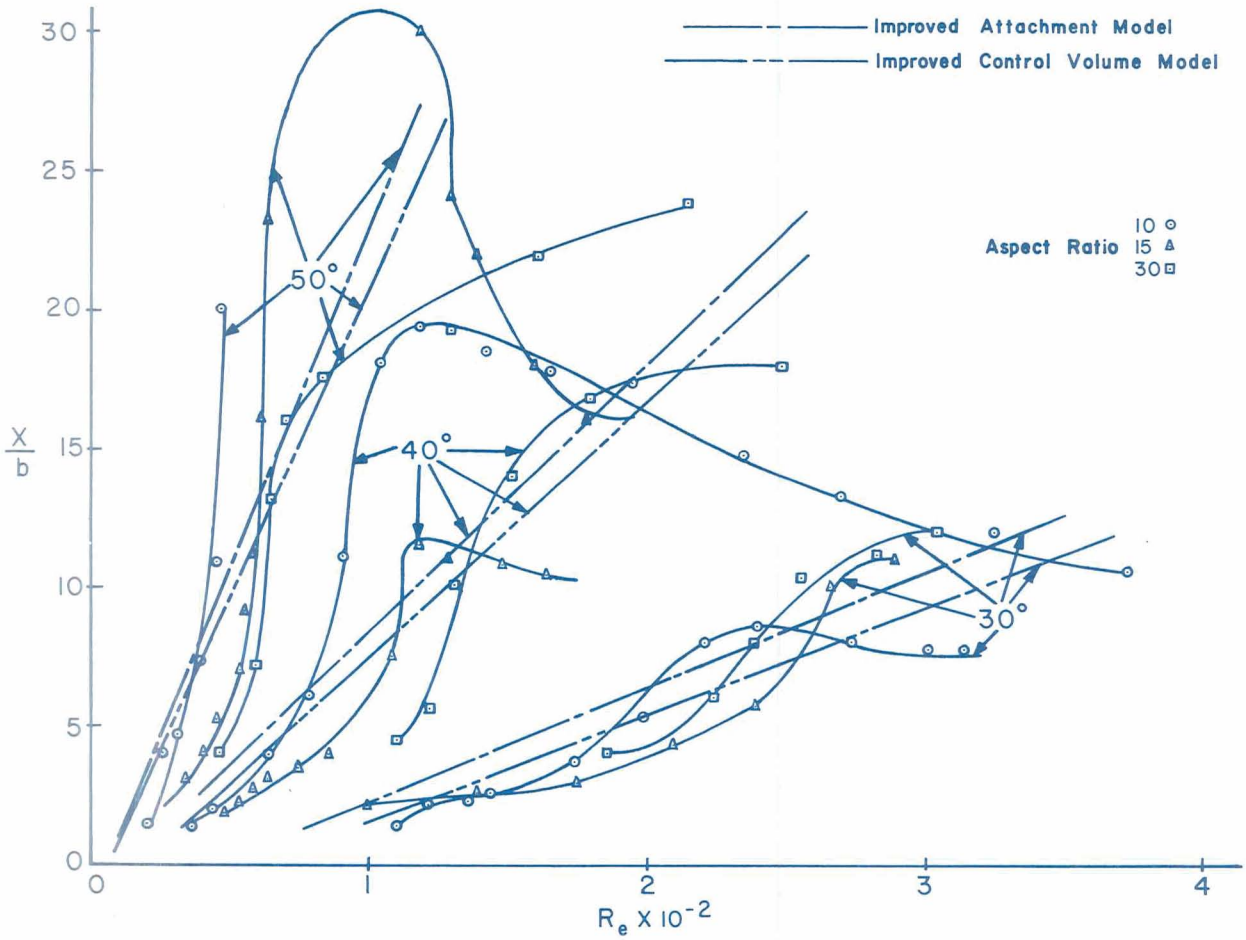

Fig. 11 Comparison of Improved Control Volume and Improved Attachment Point Models with Experimental Attachment Distances

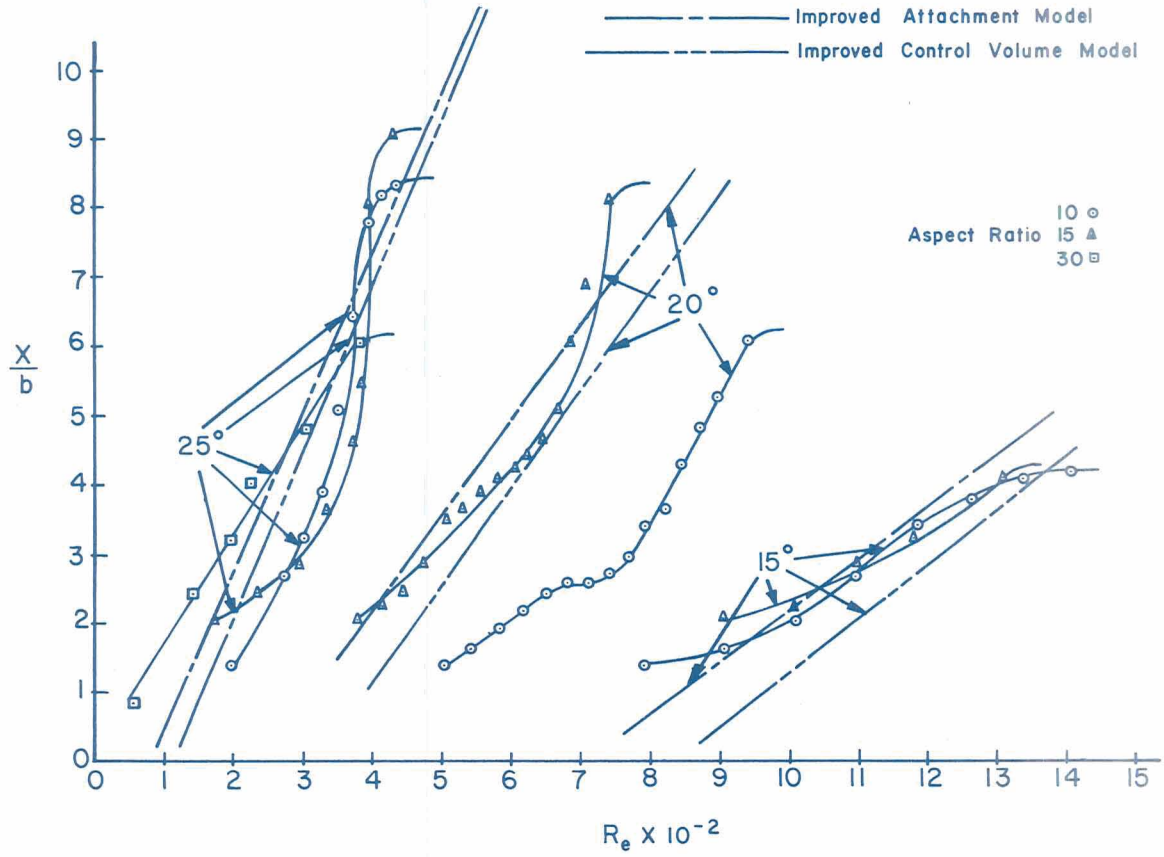

Fig. 12 Comparison of Improved Control Volume and Improved Attachment Point Models with Experimental Attachment Distances

WATER TABLE STUDY OF A MECHANICALLY DEFLECTED HYDRAULIC JET VALVE

S. A. Norén, Visiting Professor in M. E.

In servovalves of the area-controlled type (spool or flapper valves) the flow is modulated by varying the cross-sectional area of a throttling flow passage. To control small rates of flow requires small throttle areas with an inherent susceptibility to fluid contamination. This leads to high demands on filtering, and care must be taken to overcome unpredictable excess control forces. The jet type valve is a valve with a supply nozzle having a constant cross-sectional area corresponding to the maximum rate of flow needed. This means less susceptibility to contamination. Although the jet-pipe valve has been known to the engineer for more than 80 years, it is only very recently that an increasing interest in jet-type valves with mechanical control input has been shown, presumably due to recent developments in fluidics.

Figures 13a, 13b, and 13c illustrate schematically the structural differences between the jet type valves discussed here.

In Fig. 13a the jet is moved from one opening of the receiver to the other by traversing the supply nozzle relative to the receiver ports. Either of the elements can be movable while the other is stationary. This jet pipe valve is of the movable pipe type.

An example of the opposite arrangement with a stationary nozzle and a movable receiver or splitter is given in Reference [23].

Both supply nozzle and receiver are stationary in the designs of Fig. 13b and 13c. In Fig. 13b the jet is deflected by interaction with a specially shaped movable mechanical device -- a moving deflector. To this class belongs a recent development with a nozzle-like deflector, Reference [24].

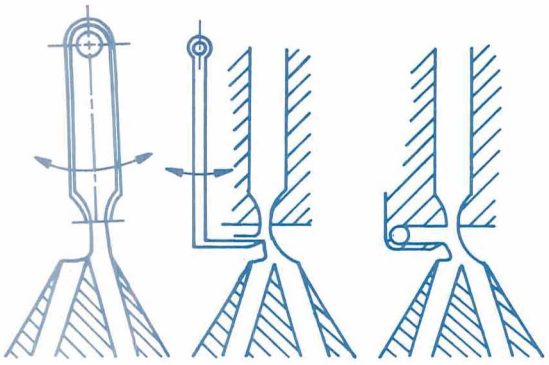

Fig. 13 Jet Deflection by Means of (a) Movable Pipe, (b) Movable Deflector, and (c) Fluid Momentum Exchange or Pressure Differential

In Fig. 13c, the deflection is accomplished without the aid of any moving parts, e.g., it is deflected by fluid momentum and/or pressure control.

Today the jet pipe valve is predominately being used as the first stage in an electrohydraulic two stage servovalve with a spool in the second stage. In that application the continuous maximum rate of flow through the valve is not a great disadvantage because of the low magnitude of the pilot power compared to the power of the main valve. Being used as a main valve, the same would be true for the jet-type valve used in cases where the corresponding power would be dissipated anyway. This is the situation in some less-sophisticated applications where a constant positive displacement type pump is used together with a relief valve to provide the hydraulic power for control purposes; for instance displacement control of hydrostatic transmissions.

It was with the latter purpose in mind that the present investigation was started, although the application as a pilot valve could be a possibility as well. Compared to the straight-edge-type deflector of Fig. 13b, a deflector of the type shown in Fig. 14a theoretically seems to be advantageous in terms of displacement gain expressed as jet deflection angle α over deflector displacement y.

To determine which is best, a very simplified physical model for each of the devices has been used, which may prejudice the results somewhat. Still, it is believed that those models will give a rough indication of how those two types of deflectors stand relative to each other.

For the straight-edged device of Fig. 14b, the principle of conservation of momentum is applied. Assuming that the free stream velocities of the deflected jet and the "peeled-off" jet are equal to the supply jet velocity v, yields

$$\rho.Q_c.v = \rho.(Q_s - Q_c)\ v \sin\alpha$$

Assuming further that the deflection angles are very small so that $\sin\alpha \approx \alpha$, and $(Q_s - Q_c) \approx Q_s$ when compared to Q_c, this expression reduces to:

$$\alpha = \frac{Q_c}{Q_s} \qquad (1)$$

The final assumption to be made is that the jet is split into two flows in a way that is directly determined geometrically by the "interception effect of the control edge. Thus, we may write

$$\frac{Q_c}{Q_s} = \frac{Y}{w} \qquad (2)$$

Combining Eqs. (1) and (2) then yields

$$\alpha = \frac{Y}{w}$$

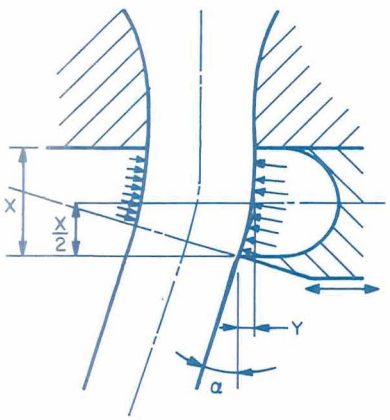

(a)

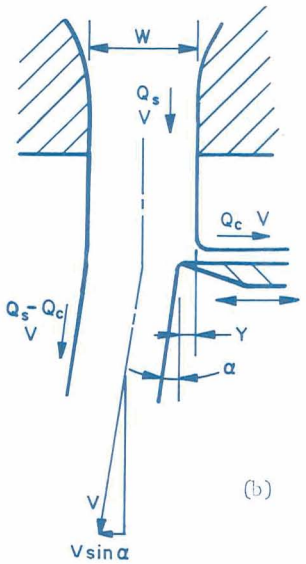

(b)

Fig. 14 Geometry and Flow Situation for (a) Cusp Type Deflector and (b) Straight-Edge-Type Deflector

As in the above case, the flow situation of the cusp-type deflector of Fig. 14a is assumed to be two-dimensional. According to the model used, it is possible for a pressure to build up in the cusp chamber. In practice this means that the deflector has to be confined by flat walls on each side. Assuming now that no momentum exchange takes place between the jet and the cusp chamber, the jet will be deflected by the pressure differential across the jet only. If this pressure differential is assumed constant along the jet in the cusp region, the jet will take the form of a circular arc. From purely geometrical reasons, it then follows that for small values of α:

$$\alpha = \frac{y}{x/2} \qquad (4)$$

If the cusp length x is equal to the nozzle width w, the expected deflection angle will be twice as great for the cusp deflector as compared to the straight-edge-type with the same deflector displacement, thus:

$$\alpha_{cusp_{x=w}} = 2\,\alpha_{(straight\text{-}edge)}$$

This possible improvement over the straight-edge deflector, and the fact that with the cusp-type deflector no net flow rate is taken from the supply jet for deflecting it, provided the incentive to carry on further investigations as to the practical applicabilities of this new type of deflector. ("Peeled-off flow" and its associated momentum is reintrained from the cusp chamber.)

Experiments were carried out on a water table with the aim of determining the actual jet deflection angle as a function of the deflector displacement. The experimental model is shown on the photograph of Fig. 15. The deflector was displaced by a positioning screw traveling .025 in. per turn. On the top cover was engraved a scale in degrees enabling the deflection angle to be determined either by observing the jet directly, as dye was injected into the supply nozzle, or by indirectly measuring the total pressure by traversing a probe across the jet. The probe was pivoted at the exit of the deflector.

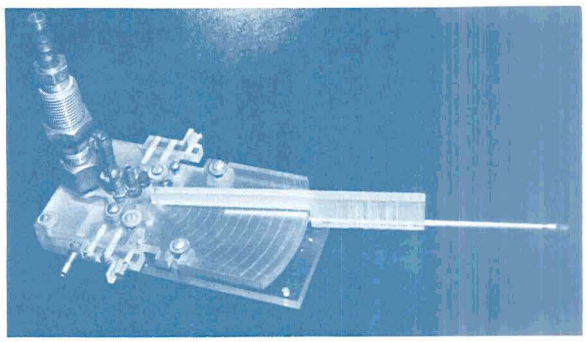

Fig. 15 Experimental Mechanical Jet Deflector Valve Model for Water Table Studies

Figure 16 shows the four basic deflector configurations tested and discussed in this report. These are designated as "open" configurations here because the 0.04 in. passage between the supply nozzle and the cusp member is open.

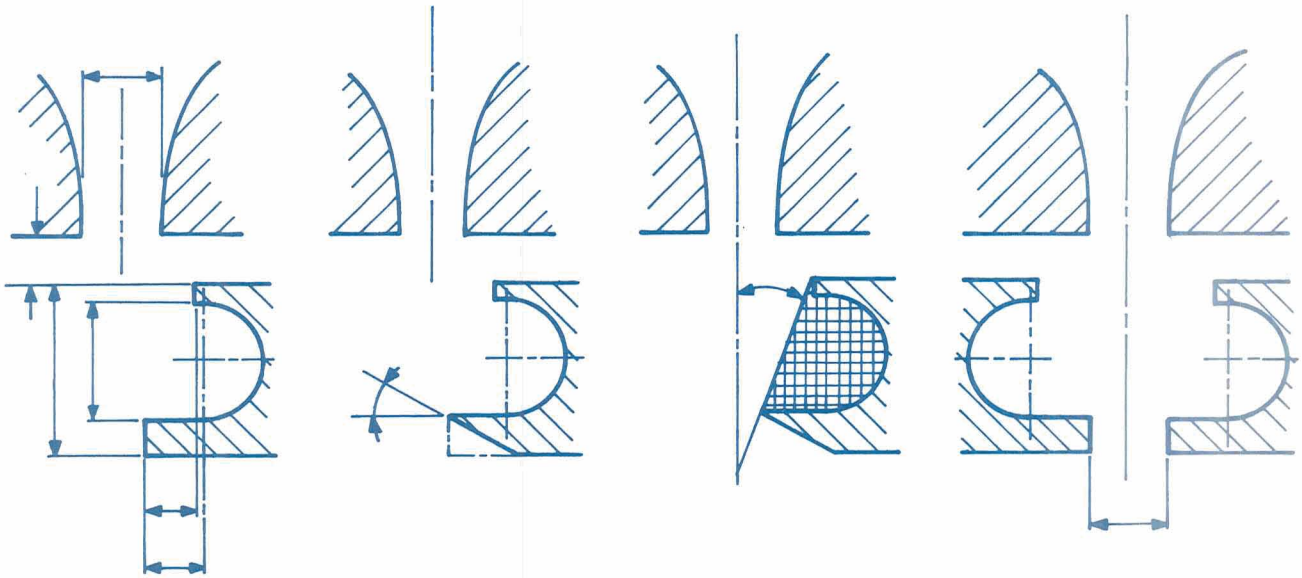

Fig. 16 Dimensions of the Four Basic Deflector Configurations. All Configurations have Supply Nozzle Aspect Ratio of 2.18

Additional configurations tested were:

Ab: as in A but with .040 in. passage blocked

Bb: as in B but with .040 in. passage blocked

Cb: as in C but with .040 in. passage blocked

AA2b: as in AA2 but with .040 in. passage on each side blocked

Test curves for the single-sided basic configurations are shown in Fig. 17. A remarkably steep increase in deflection angle takes place for the two single-cusp type configurations A and B. During the second half of the stroke the jet deflects twice as much as during the first half of the stroke. A quite different characteristic is shown for configuration C, in which the cusp is eliminated to form a flat deflection surface with an inclination of 22° to the jet axis.

Also noticeable is the effect of chamfering the downstream edge of the deflector. Apparently, some wall effect is present in configuration A which has been eliminated in configuration B.

For the same basic configurations, but with blocked passage between nozzle and cusp member, the corresponding curves are shown in Fig. 18. For positive deflection the basic character is mainly the same as for the unblocked case. For negative deflection, however, a greater difference compared to the unblocked case is noticeable. A long linear range of pulling capability of the jet is possible here, because the blocking of the upstream cusp chamber passage allows a subpressure to develop in the cusp chamber. This evidently involves the same edge-type attachment effect being utilized in some fluidic devices. Also, in the case with Bb and Cb, the displacement gain within the linear range increased by 60% over that of configuration Ab. The left dashed straight line represents the curve that should apply according to Formula (4). The simple theory presented does not appear to fit too well, although for configuration Ab some points at the end of the positive deflector stroke come fairly close to the theoretical curve. For comparison, the curve according to Formula (3) is also plotted (valid for small deflection angle for the straight-edge deflector). It is surprising that the linear region of all curves fits much better to this straight-edge theory than to the cusp theory. A much more detailed

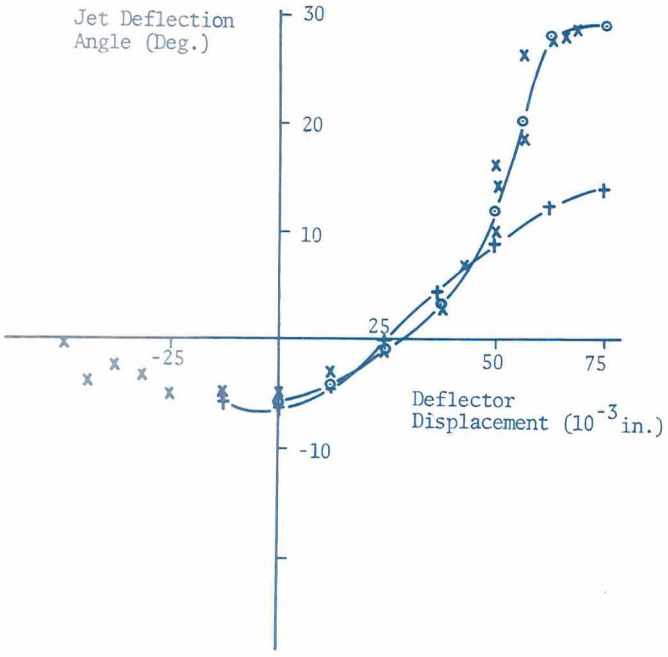

Symbol	Config.	Supply Pressure ($in.H_2O$)
x-x	A	16
⊙-⊙	B	16
+-+	C	16

Fig. 17 Jet Deflection Angle vs. Deflector Displacement for the Three Basic Open Configurations

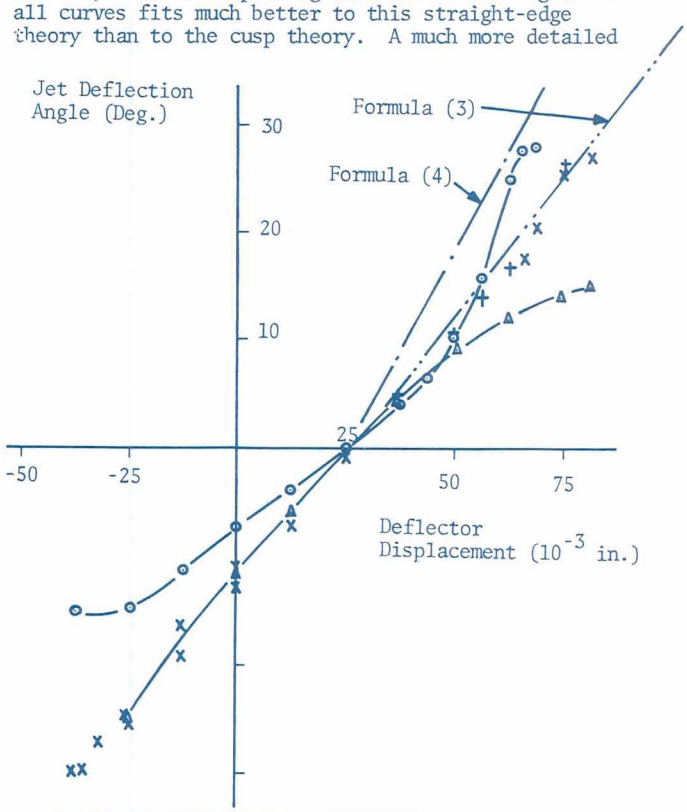

Symbol	Config.	Supply Pressure ($in.H_2O$)
⊙-⊙	Ab	16
x-+		16
Δ-Δ	Cb	16

Fig. 18 Jet Deflection Angle vs. Deflection Displacement for the Three Basic Blocked Configurations

theoretical approach seems to be necessary in order to be able to predict the performance more correctly. Figures 19, 20, and 21 show a comparison between the open case and the blocked case for the three basic configurations, A, B, and C respectively.

In particular, Fig. 19 shows the results of an investigation of the pulling capability of the deflector configurations A and Ab for which extended tests were made in the negative deflector displacement region. To fully reveal the blockage effect without introducing uncertainties such as bad repeatability in deflector position, an easily removable blocking member was used. This made it possible to observe the two modes for a given deflector setting by merely putting in place and removing the blocking member.

Figure 19 shows the results of this test. The collapse of the pulling capability of the blocked passage case takes place when return flow into the cusp starts occurring past part of the downstream edge of the deflector. That the deflection angle gets positive for large negative displacement, although it should tend to zero, depends on the particular design of the experimental model, by which the engraved jet deflection angle scale and the pivoting point of the pressure probe moves with the deflector. The diagrams have not been corrected for this error, serving so far only as a means for comparison. The dashed line 0-0 of Fig. 19, however, calculated for the probe in the position 1 in. downstream of the deflector, shows the true zero deflection angle line.

In contrast to the characteristics for the two single cusp configurations of Figs. 19 and 20, that of configuration C of Fig. 21 does not depend on whether the 0.04 in. passage between nozzle and cusp member is open or blocked for positive deflection angles; e.g., when the deflector is pushing the jet. In the negative jet deflection region (the pulling region), however, the difference in character for open and blocked case is mainly the same for all three basic configurations in that the pulling capability gets gradually lost for the open case.

Figure 22 shows the open and blocked case for two symmetrically arranged A type deflectors 0.112 in. apart, e.g., practically the same width as the supply nozzle. Compared to the same deflector used singly, Fig. 19, it can be noticed that the difference between blocked and open upstream cusp passage is exaggerated for the double deflector case. The difference is mainly in that the blocked case shows a more linear characteristic for the double deflector situation compared to the single case.

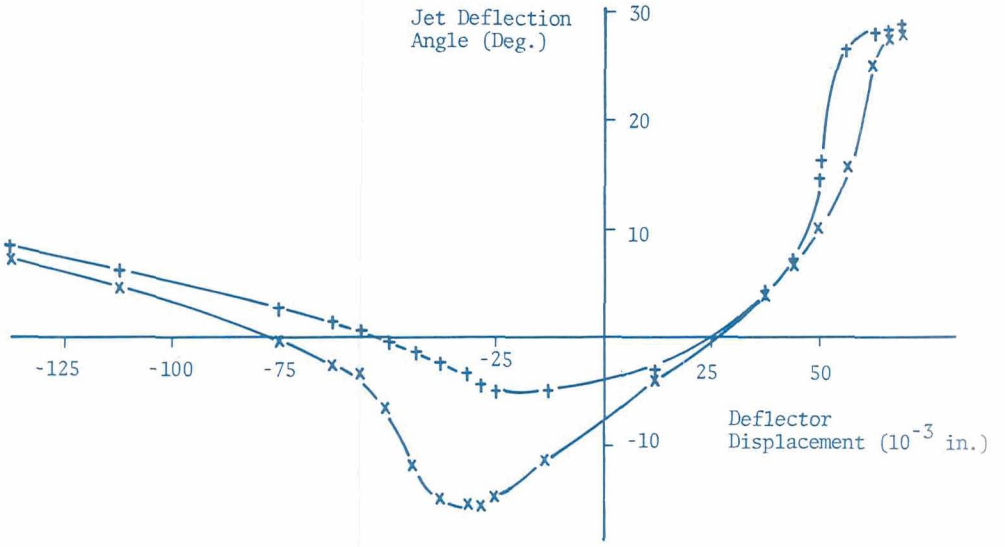

Symbol	Config.	Supply Pressure (in.H_2O)
+	A	16
x	Ab	16

Fig. 19 Jet Deflection Angle vs. Deflector Displacement for Open and Blocked Configuration A

Finally, a range of tests were made in order to investigate very roughly any Reynolds number effects on the results. Figure 23 shows a set of curves for the Bb configuration taken with supply pressures of 16 in., 1.6 in., and 0.08 in. water column. The corresponding Reynolds numbers based on nozzle width and calculated loss-free nozzle velocity are 7850, 2480, and 560 respectively. For the last pressure, the flow was purely laminar while for the first two pressures it was turbulent. Noticeable is that the pulling capability is lost very quickly in the laminar case. It is rather difficult to explain the discontinuity at -7° for the 1.6 in. run. A similar tendency can be observed for the laminar case at 17° near the saturation point. This could be a very disturbing occurrence in a practical application and the cause of these discontinuities should be thoroughly investigated.

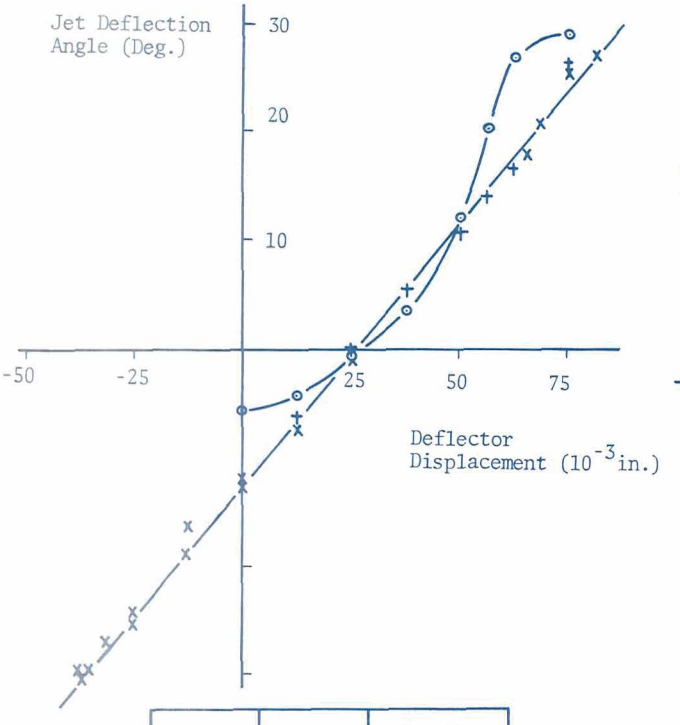

Symbol	Config.	Supply Pressure (in.H_2O)
⊙-⊙	B	16
x-+	Bb	16

Fig. 20 Jet Deflection Angle vs. Deflector Displacement for Open and Blocked Configuration B

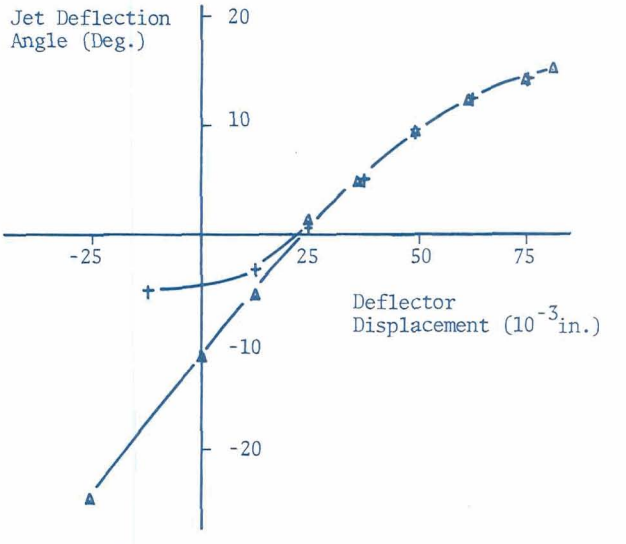

Symbol	Config.	Supply Pressure (in.H_2O)
+-+	C	16
▲-▲	Cb	16

Fig. 21 Jet Deflection Angle vs. Deflector Displacement for Open and BLocked Configuration C

This investigation clearly reveals the wide possibilities existing to influence the jet deflection characteristic by changing the geometry of the deflector. In practical application, however, it is the shape of the relationship of output pressure to deflector displacements that is of main interest. One important future step of development is therefore to arrange for an experimental model with proper receivers. By means, thereof, a systematic investigation can be carried out in order to find out how the pressure/displacement characteristic can be influenced by the geometry of the deflector.

To gain experience from the problems to be met within an actual oil hydraulic application, an electrohydraulic valve of the AA type of deflector has been built using an existing Atchley sliding plate electrohydraulic servovalve as the basic mechanism, Fig. 24. Tests with the valve will shortly be started as The Royal Institute of Technology, Stockholm, Sweden.

This project received minimal support from NASA Grant NGL 39-009-023.

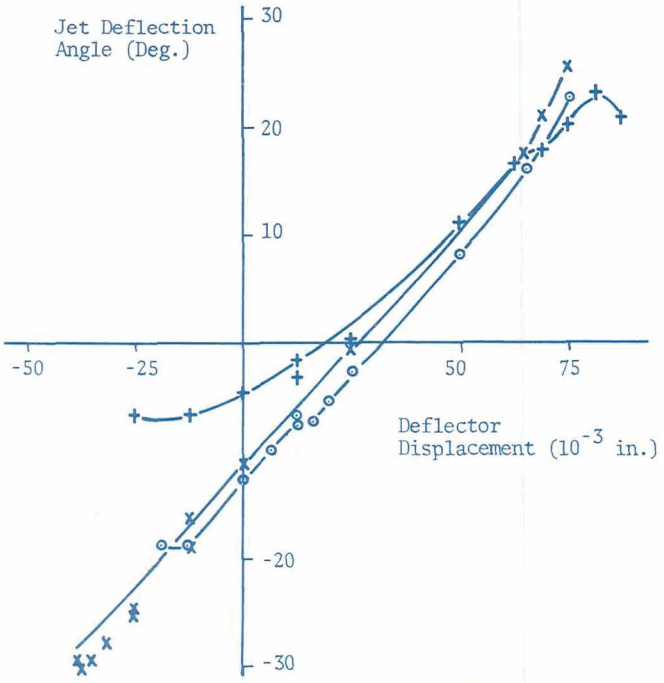

Symbol	Config.	Supply Pressure (in.H_2O)	Reynolds Number
x-x	Bb	16	7850
⊙-⊙	Bb	1.6	2480
+-+	Bb	0.08	560

Fig. 22 Jet Deflection Angle vs. Deflector Displacement for Open and Blocked Configuration AA2

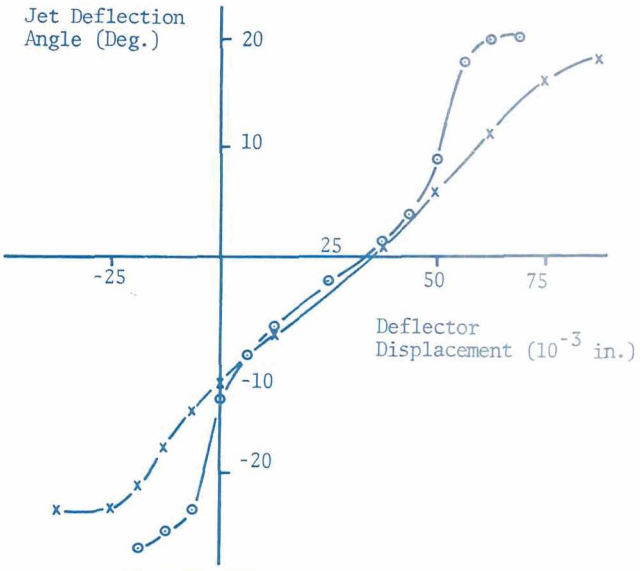

Symbol	Config.	Supply Pressure (in.H_2O)
⊙-⊙	AA2	16
x-x	AA2b	16

Fig. 23 Jet Deflection Angle vs. Deflector Displacement for Blocked Configuration B with Varying Supply Pressure

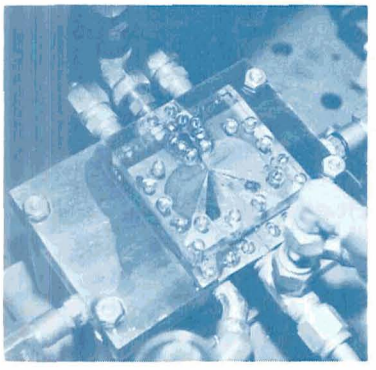

Fig. 24 Experimental Mechanical Jet Deflector Valve Model for Hydraulic Oil

MODELING OF FLUID AMPLIFIERS

A. J. Healey, Assistant Professor of M. E.
D. F. Kerstetter, Undergraduate Assistant

Phase or frequency modulated signal detection can be accomplished utilizing the frequency characteristics of amplifiers and rectifiers. This technique can provide miniaturization of detection circuits, but demands a thorough understanding of device dynamics. The special effects of geometric design must be defined in the quantitative manner that comes from a comprehensive mathematical model.

The behavior of the incoming power jet and the flow impinging on the receivers and rebounding out through the side vents are the main interests in this research project. The solution of the equations that define the flow within the fluid amplifier is done on the digital computer. These results can be compared with those taken from the large model amplifier using air that is providing physical data (see A. Knopp report -- this page).

The first method used to define the flow field within the fluid amplifier was the finite difference solution of the potential flow equation. This technique defines the flow streamlines in terms of a grid made up of node points two-dimensionally spaced over the flow field. An over-relaxation method has been used to solve for the value of the stream function at each node by the digital computer. Thus, the streamlines can be mapped over the flow pattern. Boundary conditions, however, are not known a priori and three different side vent velocity profiles were arbitrarily chosen and the receiver was assumed to be totally blocked.

The main area of interest was to determine the sensitivity of the model to boundary conditions and to see if this method could be made to predict flow separation at sharp corners in the fluid amplifier and along the walls near the power jet. The answer to this was found to be no. Basically, the reason was that a discontinuity in the flow pattern cannot be defined unless its exact nature and location is known. This method does show that the flow bends around corners and the streamlines break down at the corners and along the walls, but it does not give an exact location of the areas of flow separation which is needed.

The second method of defining the flow field around the fluid amplifier receivers was to use a control volume approach with the use of cowl streamline techniques. The case considered was that of a fluid amplifier having two receivers and two side vents. The power jet was first considered to be centered on the spike of the receivers, and afterwards to be deflected toward one of the receivers. Simpson's velocity profile [25] defined the distribution of the jet; inviscid flow is assumed, and the receivers were blocked partially or fully.

Once the control volume has been defined, the inviscid flow equations of momentum, energy and continuity, assuming two-dimensional flow, can be calculated by digital computer. Such data as receiver pressures, flow rates, rebounding jet angles, and receiver blockage were computed when the flow was defined in terms of the jet profile distribution and the cowl streamlines.

The results show that the recovered pressures in the receivers are somewhat higher than those measured experimentally by A. Knopp. One reason for this is that the mathematical model does not include energy losses of the fluid itself. Thus, a correlation must be made between experimental data and the amplifier mathematical model in terms of a loss factor to include real frictional losses. The angles of the rebounding jet out of the side vents are among the calculations, and they show some interesting results. Observed experimentally on a water table amplifier model, the rebounding jet (spillover flow in the side vents) oscillates at some particular power jet deflection from centerline. The mathematical model also predicts that the angles of the rebounding jets become undefined at certain power jet deflections. Also, the receiver widths play an important role in recovering larger receiver pressures, and in determining when the flow out of the side vents becomes unstable. To this date, an attempt to correlate experimental data with the results of the mathematical model research is being made.

This research has been supported by Contract No. DAHC04 69 C 0083 from the Army Research Office, Durham, N.C.

INVESTIGATION OF JET-RECEIVER INTERACTION EFFECTS ON PRESSURE AND FLOW RECOVERY CHARACTERISTICS OF FLUIDIC DEVICES

A. A. Knopp, Graduate Fellow in M. E.

One area of concern in the study of fluidic devices is the problem of predicting receiver recovery pressure and flow for various designs and operating conditions. Knowledge of receiver recovery pressures and flows is necessary because it determines the output signal level, the gain of the device and its effect on the dynamic behavior of the device. Although current information is available concerning the prediction of recovery pressure and

flow in large-scale diffusers, the information is not entirely applicable to fluidic devices because of the presence of two receivers in close proximity to each other and the non-uniform velocity profile which impinges upon them.

Simpson [25] has presented a theoretical method for predicting receiver recovery pressure and flow which takes into account the non-uniform velocity profile which commonly impinges upon receivers. Simpson's model is based upon the assumption that the free-jet velocity profile of the power jet is unaffected by the addition of receivers. Blocked-load pressure recovery is estimated from an integration of the free-jet total pressure profile over an area equal to the receiver entrance area and at an axial location corresponding to the receiver entry location. Similarly, open-load flow recovery is estimated from an integration of the free-jet flow at the same location.

For a given velocity distribution, Olson and Camarata [26] have shown that the flow entering the receiver may be either less than, or greater than, that portion of the jet profile intercepted by the receiver. Their data and data presented by Kallevig [27]showed that the pressure acting on blocked receivers was well predicted by Simpson's model. Reid [28], however, has pointed out that for certain ranges of geometric receivers and operating conditions, particularly for wide receivers and high blockage simple free-jet integration techniques are inadequate for estimating receiver pressure and flow recovery.

This project is primarily concerned with the investigation and prediction of receiver recovery pressure and flow in a fluidic rectifier (one receiver) operating under various loading conditions, with particular emphasis on the character of the secondary jets associated with receiver spillover flow in the vent regions. It is believed that, and preliminary experimental observations have suggested that these secondary jets, comprised of that portion of the power nozzle flow not intercepted by the receivers, can have a pronounced affect on receiver pressure recovery, flow recovery, and overall dynamic behavior of the device.

Figure 25 shows the large scale experimental model of a typical fluidic rectifier, utilizing air as the working fluid, which has been fabricated. Important features of the model include provisions for varying receiver width, receiver centerline offset with respect to the nozzle, and receiver loading conditions. In order to determine the characteristics of the flow in the vent areas, a lathe traversing mechanism has been set up to position hot wire anemometer probes in these areas.

A considerable amount of experimental data in the form of receiver spillover flow velocity profiles, together with receiver pressure recovery and flow information has been gathered. These data represent a wide variety of testing conditions in which receiver width, centerline offset, and loading were varied.

Presently, work is underway to formulate a digital computer program designed to analyze the vent spillover flow data. Characteristics such as flow direction, magnitude, jet width and spreading effects will be determined.

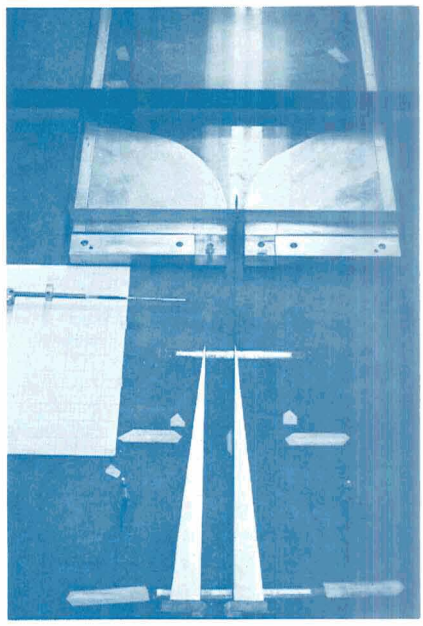

Fig. 25 Photograph of Jet-Receiver Apparatus

This research has been supported by the Army Research Office, Durham, and Union Carbide Corp.

REPORT ON SUMMER TERM IN STOCKHOLM, SWEDEN, 1970

J. L. Shearer, Rockwell Professor of Engineering

During my second term of Sabbatical leave from regular duties at The Pennsylvania State University, I accepted an invitation from the Swedish Committee for Fluidics to work in Stockholm during the Summer Term 1970.

Office space was provided in the Institution for Fluid Technology at the Royal Institute of Technology (KTH), where excellent technical library facilities were available.

During this period time was spent mainly in an advisory capacity, with research projects at KTH and at the Defense Research Establishment (FOA); independent library research was carried out; and a number of visits were made to other research activities near Stockholm and in Västerås, Göteborg, and Lund.

The main contacts at KTH were with Mr. Ingemar Skoog, Mr. Bengt Carlnäs, and Prof. Bernt Griverus. At this time Mr. Skoog was deeply involved in experimental work on a small vortex amplifier and he was extending some earlier work done by Addy and Foster at KTH on hydraulic fluid amplifiers. He was keenly interested in solving control port problems in the vortex device, and he had started to extend the results of A. K. Simson (in a Ph.D. thesis which I had supervised at M.I.T. in 1962-63), to the case of proportional fluidic amplifiers operating with hydraulic oil instead of air.

Approximately one day per week was spent at FOA with Mr. Staffan Quensel and his colleagues, H. C. Kierkegaard and Lars Strömberg, who were implementing a breadboard version of a fluidic self-optimizing system -- somewhat along the lines of the fluidic optimizer that was evolving from a Ph.D. thesis by Mr. Roger Mayne in the Systems and Controls Laboratory at Penn State. Also, a brief period was spent with Mr. Eskil Ulén to become acquainted with the development of pneumatically-operated elbow-joint mechanism which is part of an overall program at FOA to develop prosthetic devices for disabled persons.

At another part of FOA, problems associated with the occurrence of swirling flow in choked nozzles were discussed during a brief visit with Messrs. René Renström and Nils Erik Gunners.

Visits were also arranged at Atlas Copco in Stockholm, Aeronautical Research Institute (FFA) in Bromma (2 visits), Institute of Semiconductor Research (HAFO) in Vällingby, Swedish General Electric Co., (ASEA) in Västerås, Chalmers Institute of Technology in Göteborg, and Lund University near Malmö.

At Atlas Copco, accompanied by Bength Carlnäs, projects were observed with fluidic logic control of a heat-treating process and of multi-station drilling operations, and we saw a demonstration of remote control of a large pneumatic motor, a problem in which distributed parameter line dynamics play a key role.

At FFA a rather wide variety of projects were in various stages of completion and a thorough demonstration was made of their techniques for etching laminates for fluidic amplifiers. A fluidic temperature sensor with a pulse-rate output proportional to frequency had proven to be feasible and a project dealing with a new type of diverting valve showed great promise, providing excellent pressure recovery at the outputs. Technical discussions on many topics were carried on with Messrs. S. Bahrton, Göran Lundström, and K. S. Nyström, of whom the latter two were preparing for a trip to Japan. We also discussed some of the contacts I had made in Japan when I was there in the Fall of 1969.

At ASEA, accompanied by Ingemar Skoog and Bengt Carlnäs, the group was met by Mr. Per Fryklund who introduced us to Mr. Bengt Kredell, Director of Central Research and Development, and Dr. Arne Sundstrand, Manager of Mechanical Systems and Components. During the day we saw and discussed some of their work on fuel cell systems; AF hydraulic power transmission systems (4 phase); computer analysis of rotating critical speeds of shafting and of pipeline flows; and design of a large aero-medical centrifuge (for astronaut training).

At HAFO, accompanied by Mr. Staffan Quensel, discussions were held with Mr. Per Svendberg about some possibilities for development of ultra-miniature pressure transducers. They were interested in applications to medical research, miniature microphones for communications, and to fluidics research; and they had done some exploratory thinking about the possible use of small rings or diaphragms of polyimide film with vacuum deposition of gold to form pressure-sensitive electric bridges of very small size. The notion of developing a solid state sensor and electronic amplifier in a single integrated circuit did not seem to be very attractive to them. Their current lines of activity were research, development and production of semi-conductors, light-sensitive phototransistors, light-emitting diodes, integrated circuits, miniature relays, etc.

At Chalmers, accompanied by Bengt Carlnäs, a visit was made with the Fluid Dynamics Research Group of Prof. N. Frössling, where considerable talent and effort were being devoted to the solution of the Navier-Stokes equations in different fluid flow situations, including bi-stable fluid amplifiers. Laboratory facilities were still in the process of installation in a new laboratory space and some new facilities were not yet ready so that there were not many experimental projects operational on the day of our visit. A water channel had been set up for boundary layer studies; one subsonic wind tunnel was ready and another was on its way; and a new supersonic blow-down system was started. Wall-attachment studies, including turbulence measurements had been started. There seemed to be some likelihood of interaction occurring with the work by Lundström at FFA on the fluidic temperature sensor project.

At Lund University, accompanied by Bengt Carlnäs, a visit was made with Prof. Gunnar Tyllered where we saw many laboratory facilities in the final stages of construction. For their fluidics work they were building a rather elaborate water table facility for large scale model studies of fluidic phenomena. Mr. Leif Hallgren was very helpful in explaining some of their future plans and in making detailed arrangements for my lecture to a group of about 15 people.

My visit to Stockholm was well-expedited by my official host, Staffan Quensel; by Prof. Bernt Grivérus, who was acting for Prof. Anders Norén in charge of the Fluid Dynamics Department at KTH; and by Mr. Thorvald Persson (who unfortunately was on sick leave) and Eskil Ulén of FOA who have been good hosts on earlier visits by me to Stockholm as well.

For further information about the projects mentioned in this report of the activities of the Systems and Controls Laboratory, inquiries should be addressed to: Director, Systems and Controls Laboratory, 214 Mechanical Engineering Building, University Park, Pa. 16802.

LIST OF REFERENCES

1 - 11 Research Report Nos. 1 - 11, Systems and Controls Laboratory, The Pennsylvania State University, Semi-Annual Reports, April 1965-April 1970.

12. An Analytical and Experimental Study of the Influence of Swirl on Choked Nozzle Flow, T. D. Gillespie, Ph.D. Thesis, The Pennsylvania State University, December 1970.

13. Modeling Surges in Liquid Filled Lines, R. R. Huber, M. S. Thesis, The Pennsylvania State University, March 1971.

14. Linear Transient Analysis, E. Weber, v. 2., John Wiley and Sons, Inc., 1956.

15. "Fluid Transmission Lines", K. N. Reid, Notes Prepared for a Special Summer Course in Fluid Power Control, Dept. of Mech. Eng., M.I.T., Cambridge, Mass., July 1966.

16. Fluid Power Control, J. F. Blackburn, G. Reethof, and J. L. Shearer, M. I. T. Press, Cambridge, Mass., 1960.

17. A Simplified Model for a Fluid Transmission Line, R. G. Leonard, Ph.D. Thesis, The Pennsylvania State University, June 1970.

18. "A Multi-Dimensional Self-Optimizing Control System Involving Dynamics and Disturbances Employing Relay Extremum Control", G. Broekstra, C. Verhagen, and J. van Arkel, Proceedings of the Second IFAC Symposium on the Theory of Self-Adaptive Control Systems, Instrument Society of America, 1966.

19. Study of Simple Extremum Controllers Emphasizing Fluidic Implementation, R. W. Mayne, Ph.D. Thesis, The Pennsylvania State University, March 1971.

20. "Jet Reattachment at Low Reynolds Numbers and Moderate Aspect Ratios", R. A. Comparin, R. B. Moore, Jr., and W. C. Jenkins, ASME Publication No. 67-FE-25, New York, 1967.

21. "Fluid Amplification Five, Jet Attachment Distance as a Function of Adjacent Wall Offset and Angle", S. Levion and F. M. Manion, Harry Diamond Laboratories, Report TR-1087, Dec. 1962.

22. Boundary Layer Theory, H. Schlicting, McGraw-Hill Book Co., Fourth Edition, 1960.

23. "Fachausstellung und Fachtagung Servotechnik", Dipl.-Ing. Hans Esch, Monchenbach, Ölhydraulik und Pneumatik 14 (1970) Nr 9, p. 399.

24. The Deflector Jet Servovalve, Technical Bulletin 121, Moog Inc., East Aurora, N.Y. 14052.

25. A Theoretical Study of the Design Parameters of Subsonic Pressure Controlled Fluid Jet Amplifiers, A. K. Simson, Ph.D. Thesis, Massachusetts Institute of Technology, July 1963.

26. "Pressure Recovery Characteristics of Compressible Two-Dimensional Free Jet Flows", R. E. Olsen and J. F. Camarata, Proceedings of the Fluid Amplification Symposium, October 1965, Vol. 1, H.D.L.L

27. "Effect of Receiver Design on Amplifier Performance and Jet Profile of a Proportional Fluid Amplifier", Proceedings of the Fluid Amplification Symposium, October 1965, Vol. 1, H.D.L., J. A. Kallevig.

28. Static and Dynamic Interaction of a Fluid Jet and a Receiver Diffuser, K. N. Reid, Sc. D. Thesis, Massachusetts Institute of Technology, September 1964.